Energy Reports 8 (2022) 12117–12125

Contents lists available at ScienceDirect

Energy Reports

journal homepage: www.elsevier.com/locate/egyr

Research paper

Multi-form heat storage performance of expanded graphite based $CaCl_2$ composites for low-grade heat source

Na Gao [a,b], Lisheng Deng [a,c], Jun Li [a], Hongyu Huang [a,c,*], Bin Zhou [d], You Zhou [d,**]

[a] Guangzhou Institute of Energy Conversion, Chinese Academy of Sciences, Guangzhou 510640, China
[b] University of Chinese Academy of Sciences, Beijing 100049, China
[c] Southern Marine Science and Engineering Guangdong Laboratory (Guangzhou), Guangzhou 511458, China
[d] National Institute of Clean-and-low-carbon Energy, Beijing 102211, China

ARTICLE INFO

Article history:
Received 30 May 2022
Received in revised form 10 August 2022
Accepted 12 September 2022
Available online 26 September 2022

Keywords:
Expanded graphite
Calcium chloride
Composite
Multi-form sorption
Thermal energy storage

ABSTRACT

Hydrated salt $CaCl_2$ is a promising material for low-grade thermochemical heat storage. To improve cyclic stability of the material, porous matrixes are usually employed to synthesize $CaCl_2$/matrix composites. However, the multi-step reaction of the salt and multi-form sorption of the composites increase the complexity during the practical application. This study proposed a novel method to study the multi-form heat storage performance. By combining TG/DSC measurement with Peak-fitting analysis, the multi-form mechanism of hydration/dehydration is revealed quantitatively. A series of EG/$CaCl_2$ composites are synthesized with different salt content in the range of 23.8 wt% ~57.8 wt%. All of the composites show well endothermic dehydration performance below 130 °C. A highest heat storage density of 1637.6 kJ/kg was obtained with a salt content of 48.1 wt% and a water uptake of 0.79 g/g. Water uptake of EG/$CaCl_2$ composites is composed of chemisorption water loaded through reversible hydration reactions and solution absorption water introduced from salt deliquescence. The solution absorption plays nearly the equitant important role as chemical sorption, both in water adsorption ability and thermal storage capacity. The EG/$CaCl_2$ composite show great support capacity for both salt and solution, making it an interesting material for low-grade heat storage.

1. Introduction

During the process chain of energy conversion from primary energy carriers to final energy use, a high amount of global energy input is lost as waste heat (Forman et al., 2016). Recovery technologies of waste heat have been widely discussed to restrain growing global energy consumption. However, practical utilization of waste heat by traditional thermodynamic cycles could be limited by several problems, especially for low-grade waste heat. One of the problems is that a narrow temperature difference between low-grade heat resource and heat sink can pose a big challenge for cycle efficiency (Wolf et al., 2022). Besides, distribution of waste heat is usually intermittent and instable, causing supply–demand mismatch between waste heat provider and energy user (Ding et al., 2022).

Thermal energy storage (TES) is a promising technology to overcome these problems of waste heat recovery. In a TES system, waste heat is transformed into chemical potential through reversible reactions, and then stored in the products with an energy storage density depending on the associated reaction enthalpy (ΔH). A universal description of TES based on chemical reactions can be deduced from following general correlation (Linder, 2021):

$$Educts \leftrightarrow Product\ (s) + \Delta H \quad (1)$$

The reaction products can be easily separated, which allows long-term energy storage and long distance transportation at ambient temperature with little heat loss (Angerer et al., 2018).

Gas–solid reaction with water vapor is mostly considered due to its controllability in the pressure and reaction temperature according to the reaction's thermodynamic equilibrium (Gollsch et al., 2020). Upgrade of low-grade thermal energy is achievable in this type of TES system by adjusting the pressure during endothermic/exothermic reactions. Thereinto, hydrous salt is proved to be a potential candidate due to the simplicity of reaction, described as follows (Yan et al., 2015):

$$Salt \cdot nH_2O\ (s) + Heat \leftrightarrow Salt(s) + nH_2O(g) \quad (2)$$

* Correspondence to: No. 2, Nengyuan Rd., Wushan, Tianhe District, Guangzhou, China.
** Correspondence to: Future Science and Technology City Road, Changping District, Beijing, China.
E-mail addresses: gaona@ms.giec.ac.cn (N. Gao), huanghy@ms.giec.ac.cn (H. Huang), you.zhou.c@chenergy.com.cn (Y. Zhou).

https://doi.org/10.1016/j.egyr.2022.09.051

A wide range of hydrous salts as thermochemical heat storage materials have been discussed including $CaCl_2{\cdot}nH_2O$ (Touloumet et al., 2021), $LiOH{\cdot}H_2O$ (Kubota et al., 2019; Li et al., 2021), $MgCl_2{\cdot}6H_2O$ (Zhou and Zhang, 2022), $MgSO_4{\cdot}7H_2O$ (Calabrese et al., 2019), $SrBr_2{\cdot}6H_2O$ (Richter et al., 2018; Stengler et al., 2020), etc. Among them, calcium chloride have a great superiority owing to its low cost, environmental friendliness, high heat storage density and high reaction rate (Esaki and Kobayashi, 2020). Since $CaCl_2$ has a rather low deliquescence relative humidity (DHR) value (29% at 30 °C) (Xueling et al., 2021), which may cause particle aggregation and solution leakage of the system, porous material are normally used as a host matrix to improve the structural stability of $CaCl_2$. Various porous materials have been reported as the host matrixes such as vermiculite (Zhang et al., 2016), activated carbon (Posern and Osburg, 2018), Expanded graphite (Zamengo et al., 2015), zeolite (Wang et al., 2019), silica gel (Skrylnyk et al., 2018), anodic aluminum oxide (AAO) (Yilmaz et al., 2020), graphene (Ait Ousaleh et al., 2020), carbon nanotubes (Mastronardo et al., 2016) and mesostructured cellular foam (MCF) (Liu et al., 2022), etc. (Jabbari-Hichri et al., 2017) investigated the impact of different mesoporous supports (silica gel, alumina and bentonite) with the consistent $CaCl_2$ addition of 15 wt%, among which silica gel showed the best performance (746 kJ/kg) with a sorption capacity of 0.27 g/g. Courbon et al. (2017) attain a higher salt content of 43 wt% for silica gel/$CaCl_2$ composite and obtained an excellent energy storage capacity of 1080 kJ/kg, with a sorption capacity of 0.40 g/g. Ristić et al. (2012) proposed a new two-component water sorbent $CaCl_2$-FeKIL2 to obtain an improved water sorption capacity of 0.58 g/g and the heat storage capacity of 560 kJ/kg. Then they (Ristić and Logar, 2019) introduced $CaCl_2$ into PHTS matrix (plugged hexagonal template silicate) with concentrations: 4 wt%, 10 wt% and 20 wt%, and a highest integral heat of 1199 kJ/kg was achieved with a sorption capacity of 0.43 g/g. Touloumet et al. (2021) incorporated $CaCl_2$ into aluminum fumarate (AF) MOFs by a salt content of 58 wt% and claimed an energy heat storage capacity of 1840 kJ/kg, coupled with a sorption capacity of 0.68 g/g. After that they developed the host matrix into a hierarchical microporous/mesoporous AF/Al with a higher salt content of 61% to lift heat storage capacity to 1938 kJ/kg (Touloumet et al., 2022). It can be concluded from researches that $CaCl_2$ is a quite promising candidate for low-grade thermal energy storage, and the heat storage capacity depends strongly on boundary conditions (reaction temperature and pressure), as well as the water uploading characteristics.

A major shortcoming of the $CaCl_2$/matrix composites might be the complexity in the water sorption/desorption process. On one hand, the hydration/dehydration reaction is multi-staged, associated with the hydration number (n) in the hydrate ($CaCl_2{\cdot}nH_2O$) (Rammelberg et al., 2012), which make the process more complex. Molenda et al. (2013) analyzed systematically the hydration/dehydration behavior of pure $CaCl_2$ under high partial vapor pressures, and found the formation of $CaCl_2{\cdot}0.3H_2O$ as a stable intermediate product. Fujioka and Suzuki (2013) reported a four-step $CaCl_2/H_2O$ reaction for a $CaCl_2$-EG composite, with the intermediate products of $CaCl_2{\cdot}H_2O$, $CaCl_2{\cdot}2H_2O$, $CaCl_2{\cdot}4H_2O$, and final product of $CaCl_2{\cdot}6H_2O$. Touloumet et al. (2021) obtained the same final product obtained for $CaCl_2$ confined in AF, but followed a three-step reaction with the intermediate products of $CaCl_2{\cdot}2H_2O$, $CaCl_2{\cdot}4H_2O$. Such difference in reaction steps can be tuned by controlling the reaction temperature or pressure. The number of crystal water in the products $CaCl_2{\cdot}nH_2O$ has a major impact on the material storage density (Kimpton et al., 2020).

On the other hand, possible sorption of a composite commonly involves not only the hydration of salt, but also the physical adsorption by matrix, the exothermic dissolution by deliquescence and subsequent absorption of water by the solution into the pores. Kim et al. (2014) investigated physical adsorption and chemical reaction (period, adsorption rate, water uptake amount) of $CaCl_2$/EMC composite. Xu et al. (2019) introduced an "three-step" hydration method to measure and evaluate water uptake contributions of physisorption, chemisorption and absorption of MgCl2@zeolite composites. Nonnen et al. (2020) confined hygroscopic salts (NaCl, $CaCl_2$, $MgCl_2$, $MgSO_4$) into zeolite Na-X beads to investigated the role of deliquescence on the thermochemical properties, finding deliquescence showed positive effect to water uptake and heat storage density. However, for most of the highly hydrophilic salt, salt leakage has been a main problem that may result in degradation of heat storage performance. Moreover, melting temperatures are quite low for highly hydrated $CaCl_2$(29.9 °C for hexa-hydrate and 45.5 °C for tetra-hydrate), forming another unstable factor in utilization (N'Tsoukpoe et al., 2014; Company, 2003). Therefore, detailed researches are quite necessary on the multi-form sorption/desorption as well as clarification of intermediate products.

To the best of our knowledge, two main methods have been used in previous studies to demonstrated the complex sorption/desorption behavior of composite material: (1) dividing the single steps with specific temperature/humidity procedure; or (2) defining demarcation points on experimental curves by key parameters such as reacted fraction value or TG peaks. However, the general mechanism of multi-step dehydration has not been revealed as clear as enough, especially for the composites with high-overlapped desorption steps. Since the overlapped steps occur simultaneously, it is quite difficult to make a clear quantitative division between these steps only through experimental method.

In the present study, the peak fitting approach (Janković et al., 2018) are firstly used in heat storage field for exploring the multi-step mechanism of composites desorption. The novel method is able to separate the high-overlapped peaks in TG/DSC curves, and conveniently figure out the quantitative contribution of each peak to the total water sorption ability and heat storage capacity. Expanded graphite (EG) was applied as the matrix due to the high thermal conductivity (Ao et al., 2022; Haruki et al., 2020), high surface area (Xing et al., 2022), and high permeability and durability (Haruki et al., 2019; Miao et al., 2021). This study provides a better understanding of multi-form heat storage performance of composite materials, and reveals the key factor of performance improvement.

2. Experimental section

2.1. Preparation of composites

The composite samples were synthesized by impregnating expanded graphite (EG) (purity ≥99.9%, D50:8 μm, Suzhou Dongneng new material, Ltd.) with aqueous $CaCl_2$ (purity ≥ 96.0%, Tianjin Zhiyuan Chemical Reagent, Ltd.) solution at atmospheric pressure. EG matrix was first dehydrated in an oven at 150 °C for 8∼10 h, and then cooled down to ambient temperature before added to the aqueous solution of $CaCl_2$. The salt solution is prepared in advance using deionized water. Altogether 4 different concentrations of the solution ranging from 10% to 42% were adopted in order to get composite samples with different salt contents. After 4 hours' impregnation accompanied with stirring, the mixture was filtered by a vacuum extraction method and then dried in an oven at 150 °C for more than 10 h. Thereby the anhydrous EG/$CaCl_2$ composites were obtained. For comparison, the pure EG was also prepared by being dewatered under the same condition.

The salt content of composite, SC, is calculated by Eq. (3):

$$SC\ (\%) = \frac{m_{composite} - m_{EG}}{m_{composite}} \tag{3}$$

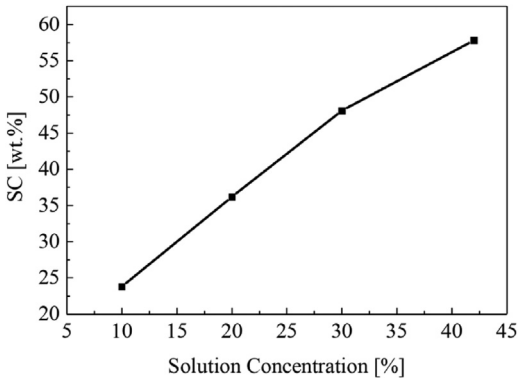

Fig. 1. SC value changes with solution concentration.

With $m_{composite}$ being the mass of an anhydrous composite, and m_{EG} being the mass of the anhydrous EG before impregnation.

Fig. 1 shows salt contents of the composites prepared from different impregnation concentration. It is seen that SC value of EG/$CaCl_2$ composite increases monotonically with concentration of the impregnating solution. A highest salt content of 57.8 wt% is reached with the solution concentration of 42%, and more than 36 wt% can be achieved when the concentration exceeds 20%. The samples are named as EG/$CaCl_2$-1 (23.8 wt%), EG/$CaCl_2$-2 (36.2 wt%), EG/$CaCl_2$-3 (48.1 wt%) and EG/$CaCl_2$-4 (57.8 wt%), corresponding to solution concentrations of 10%, 20%, 30%, 42%, respectively. Pure EG is regarded as a composite with the SC value of 0 wt%.

2.2. Apparatus and experimental procedure

Surface morphologies of pure EG and EG/$CaCl_2$ composites were observed by field-emission scanning electron microscope (SEM, S-4800, Hitachi L td.). Interior topography as well as salt loading characteristics were analyzed by Trans-mission electron microscope (TEM, JEM-2100-F, JEOL) equipped with an energy dispersive Spectrometer (EDS) for chemical compositions mapping. The specific surface area, total pore volume and pore size was derived using Mercury Instruction Porosimetry (MIP, Autopore V9600, Micromeritics Instrument Corp.) Hydration experiments were conducted in a thermostat cabinet under three constant operating mode separately: 30 °C/80%RH, 30 °C/60%RH, 20 °C/80%RH. After hydration, the composite was put into a simultaneous thermal analyzer (TGA/DSC+, METTLER TOLEDO) to investigated the dehydration behavior and endothermic effect under constant heating rate of 5 °C/min from 25 °C to 200 °C, with nitrogen as the inert gas. The experiment gas flow surrounding the sample was set to 50 mL/min.

2.3. Evaluation method

Water adsorption capacity is calculated by water uptake quantity per unit mass (Eq. (4)):

$$Wsor(g/g) = \frac{m_{hydrate} - m_{anhydrate}}{m_{anhydrate}} \tag{4}$$

With $m_{hydrate}$ being the mass of the hydrous sample in saturated condition, and $m_{anhydrate}$ being the mass of corresponding anhydrous sample.

To analyze changes in water quantity and reaction state during dehydration process (TG experiments), instantaneous water mole content ($nH_2O/nCaCl_2$) and conversion rate were introduced in this study, defined by Eqs. (5) and (6):

$$nH_2O/nCaCl_2\ (mol/mol) = \frac{W - W_s}{W * SC} * \frac{111}{18} \tag{5}$$

$$Conversion\ rate\ (\%) = \frac{W_0 - W}{W_0 - W_S} \tag{6}$$

with W being the weight at temperature T, W_0 being the initial weight and Ws being the stabled weight after dewatering process.

To reveal the multi-step mechanism of the water transformation in the EG/$CaCl_2$ composites during dehydration, the TG and DSC curves was analyzed through differential and integral methods. Peak fitting method was performed to separate and analyze the overlapping peaks of (DTG) and DSC curves. Gaussian function is applied as the model function of the overlapping peaks, as expressed by Eq. (7):

$$y = y_0 + \frac{A}{\omega * \sqrt{\frac{\pi}{4ln2}}} * exp[-\frac{4ln2(x - x_c)^2}{\omega^2}] \tag{7}$$

with y_0 being the baseline, A being the area of different sub-peaks, ω being the full width at half maximum(FWHM) of different sub-peaks and x_c being the position of different sub-peaks. Fitting analysis was carried out using Origin software. Validation of the approach was verified through integral of predicted DTG sub-peak to assess how well the calculated weight change of sub-peaks superimposed with the experimental TG curve, as expressed by Eq. (8) (Owusu-Ware et al., 2013):

$$W_T = W_0 - \int_{T_0}^{T} \left(\frac{dW}{dT}\right) dT \tag{8}$$

3. Results and discussion

3.1. Microstructure characterization

Fig. 2 show SEM images of EG matrix before (Fig. 2(a)) and after (Fig. 2(b)) being impregnated with $CaCl_2$. The matrix exhibits a lamellar structure with abundant hollow layers of a thickness around 100 nm, which could provide a good condition for salt deposition. The salt was found to be well-located between the layers of EG matrix through impregnation method, and apparent distortion of structure is not observed. TEM image (Fig. 3) and elemental mapping (Fig. 4) show a quite good dispersible homogeneity of salt in the composite. $CaCl_2$ crystal can be seen being densely packed into EG matrix, which is consistent with SEM images, and the concentrate of Ca and Cl elements are generally uniform inside the composite particles. The upload pattern of salt into EG matrix can be very helpful for reaching a relatively high salt content.

The salt loading capacity of the EG matrix is confirmed by MIP results (Table 1). The total pore volume of EG matrix decreases from 3.95 cm^3/g to 0.63 cm^3/g after impregnation, and the average pore diameter shrinks by 78% correspondingly. Assuming that difference of pore volume between pure matrix and composite is occupied by salt, the salt content can be calculated through the following equation (Courbon et al., 2017):

$$SC = \frac{V_{Pmatrix} - V_{Pcomposite}}{V_{Pmatrix} + \frac{1}{\rho_{salt}}} \tag{9}$$

With $V_{Pmatrix}$ being the pore volume of pure matrix, $V_{pcomposite}$ being the pore volume of composite, and ρ_{salt} being the density of anhydrous $CaCl_2$ (2.15 cm^3/g). According to this equation, pore volume of the EG/$CaCl_2$ should be 1.83 cm^3/g, which is larger than the experimentally measured pore volume. The main reason might be that a portion of matrix pores are blocked by salt deposition. In spite of this, high porosity (57.0%) and specific surface area (11.51 m^2/g) is retained for the composite, ensuring the mass transfer capacity and reaction interface during heat storage process.

As a porous host matrix, EG is helpful for improving the heat storage performance of pure salt through the following three

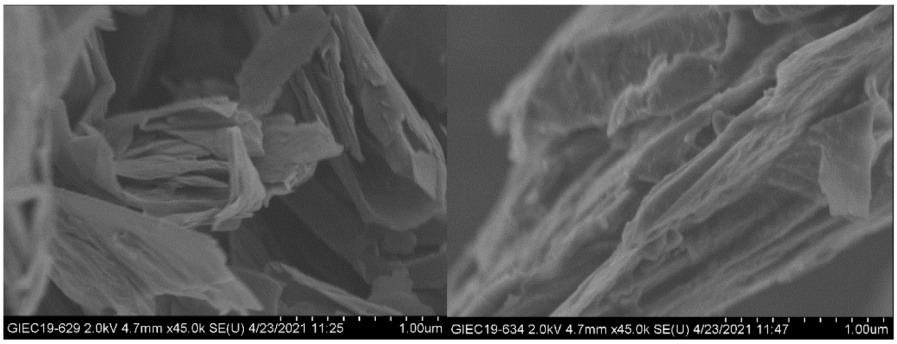

Fig. 2. SEM images of pure EG (a) and EG/$CaCl_2$-3(b).

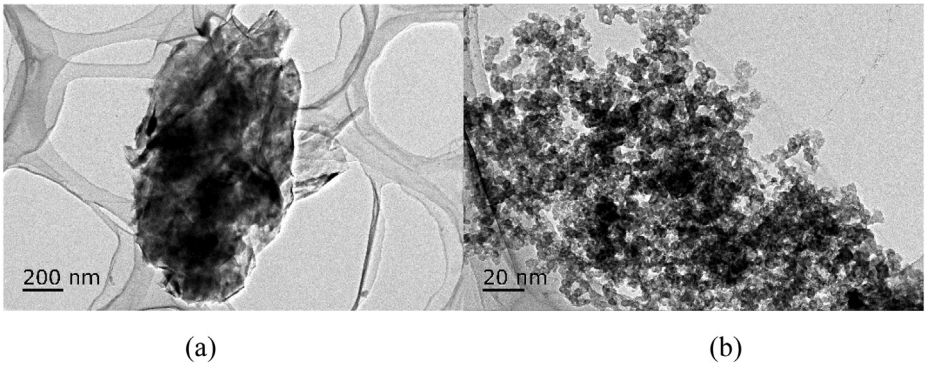

Fig. 3. TEM image of EG/$CaCl_2$-3.

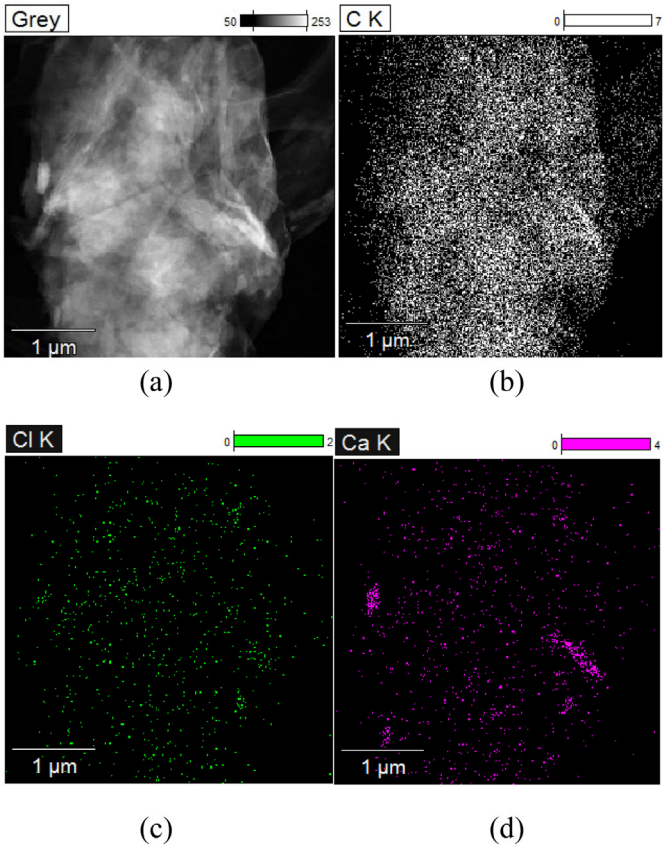

Fig. 4. Elemental mapping images of EG/$CaCl_2$-3.

Table 1
Structural properties of EG matrix before and after impregnation.

Sample	Specific surface area (m^2/g)	Total pore volume (cm^3/g)	Average pore diameter (nm)	Porosity
EG	15.97	3.95	998.84	82.1%
EG/$CaCl_2$-3	11.51	0.63	218.69	57.0%

aspects: (1) support the salt as a framework to decrease aggregation of crystal particles, thereby improve the mechanical strength and cycling stability; (2) supply room for the residence of $CaCl_2$ hydrate which guarantees a high heat storage capacity; (3) provide good porosity for transportation of steam during hydration/dehydration process for improving capacity and mass transfer performance; (4) hold the salt solution in its porous structure, reducing leakage losses that arise from deliquescence; and (5) keep liquid salt from leaching when the operation condition exceeds the melting temperatures.

3.2. Multi-form sorption

Fig. 5 shows the water absorption capacity of pure EG and EG/$CaCl_2$ composites of different salt content under three different temperature and humidity condition. For the pure EG (SC = 0 wt%), very few water ($\leq$0.02g/g) is uploaded by physisorption. Since physisorption will be restrained when there is salt loaded in the matrix because of a reduction in the available pore volume (Touloumet et al., 2021), physisorption is considered negligible for EG/$CaCl_2$ composites in this study. For low-SC samples (EG/$CaCl_2$-1, EG/$CaCl_2$-2), total water uptake increases gradually with salt content at a modulated rate. As the salt content further increases ($\geq$36 wt%), the curve gradient is lifted to a higher level, indicating the effect of solution absorption being

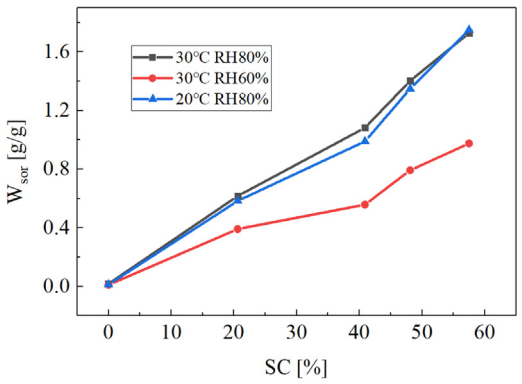

Fig. 5. Effect of salt content on water uptake capacity at different temperature and humidity condition.

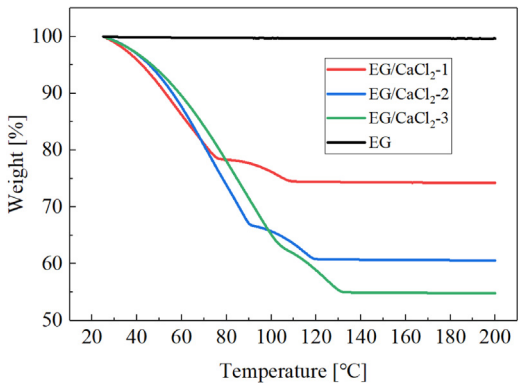

Fig. 6. TG curve of pure EG and EG/$CaCl_2$ composites.

intensified. The higher the ambient humidity, the more solution absorption would be, therefore the greater the curve gradient is. Combining chemisorption and solution absorption, a highest Wsor up to 1.75 g/g was obtained, for the sample EG/$CaCl_2$-4 under RH80% condition.

Comparing the W_{sor} –SC curves under different atmosphere, there is an interesting finding that water absorption capacity of the composites mainly depends on relative humidity of atmosphere rather than on temperature. This can be explained by the calculation of the deliquescence relative humidity (DRH) via the Raoult's law yields (Veith et al., 2021):

$$\frac{DRH_{Raoult}}{100\%} = x_{water} \tag{10}$$

with x_{water} being the mole content of saturated solution at temperature T, which could be calculated by the solubility (s) of salt:

$$\frac{DRH_{Raoult}}{100\%} = x_{water} = \frac{1}{1+\frac{s}{100}*\frac{18}{111}} \tag{11}$$

The coefficient of solubility in the formula is so small that x_{water} value changes very little while solubility increases with temperature. Since degree of deliquescence is determined by the relation between relative humidity (RH) and DRH, it can be concluded that the water uptake introduced by deliquescence mainly depends on the RH of the thermostat cabinet. As is seen in Fig. 5, temperature increasing from 20 °C to 30 °C makes a very small decrease on DRH value, thus a tiny lift on water sorption.

It is worth noting that EG/$CaCl_2$ composites exhibit strong supporting ability for aqueous solution. After a 12-h water sorption, and the samples were gradually turned into a clayey form because of agglomeration. No obvious solution leakage was observed for the samples with a water uptake less than 1.0 g/g. As the W_{sor} further increases, solution exudation was observed. This result indicates that deliquescent inside the composites may make a positive contribute to heat storage capacity in the manner of adsorption heat without the risk of heat leakage.

3.3. Multi-step desorption

Mass changes of hydrated samples during the desorption process have been studied using thermogravimetric (TG) analysis. For the sake of minimizing the effects of salt leakage, four samples (pure EG, EG/$CaCl_2$-1, EG/$CaCl_2$-2, EG/$CaCl_2$-3) processed under 30 °C and 60% RH condition are adopted in this section, in which obvious exudation of solution is not observed. According to equilibrium relationship between temperature and pressure (Fujioka and Suzuki, 2013), the final product of $CaCl_2$-hydration reaction under 30 °C 60% RH condition would be $CaCl_2{\cdot}6H_2O$.

Fig. 6 shows the normalized weight curve of the samples during desorption. It is found that the weight of pure EG remain nearly constant (weight loss < 0.5%), and weight losses of composites are 25.8% (EG/$CaCl_2$-1), 39.4% (EG/$CaCl_2$-2), 45.2% (EG/$CaCl_2$-3), respectively. The results coincide with the gross water uptake measured in sorption experiments (28.0% for EG/$CaCl_2$-1, 35.8% for EG/$CaCl_2$-2, and 44.2% for EG/$CaCl_2$-3) with an error of 2%∼9%. The deviations mainly result from difference in quantity of sample mass used in sorption and desorption processes. It is found from the TG curves that immediate weight loss happens from the very beginning of the heating procedure by a higher rate than reaction rate of chemical dehydration (Xin et al., 2022), implying that solution desorption occurs before chemical dehydration. Moreover, one can see an obvious curve break in the back segment after which a sudden drop of change gradient happens, meaning the start of another sub-step with a lower desorption rate. As the salt content increases, the turning point moves upward as well as the endset temperature. Overall, for EG/$CaCl_2$ composites, the main dehydration process can be finished within 130 °C.

Fig. 7 shows the dynamic curve of the water mole content ($nH_2O/nCaCl_2$) and conversion during the dehydration process. The initial amount of $nH_2O/nCaCl_2$ of each composite goes beyond 10, which is far more than the maximum hydration number (6) in the hydrate ($CaCl_2{\cdot}nH_2O$). This further proves that solution absorption introduced through deliquescence takes up a considerable proportion in total water uptake. It is noted that the initial water mole content of EG/$CaCl_2$-3 seems a little lower than the other samples, which might be caused by a slight solution leakage that is invisible to the naked eyes.

During the desorption process, the water mole content drops dramatically to 2 at first, and then the variation slow down till completely dry. It is evident that at the turning point, water inside the porous matrix mostly exist in the form of di-hydrate. That is to say, the slower desorption period after the turning point turns out to be a dehydration process of $CaCl_2{\cdot}2H_2O$. Comparing with the conversion curves, it is easy to find that the turning point is corresponding with a conversion of approximately 0.83 for all samples, and after that the conversion rate decreased. When temperature arrives at 120 °C, EG/$CaCl_2$-1 and EG/$CaCl_2$-2 have been completely dried, and EG/$CaCl_2$-3 reaches a conversion of 0.9. Then the latter sample approaches to a complete desorption at 130 °C.

The derivative TG curves are shown in Fig. 8. The peaks indicate that desorption of the EG/$CaCl_2$ composites involves at least three steps, including water desorption from salt solution and

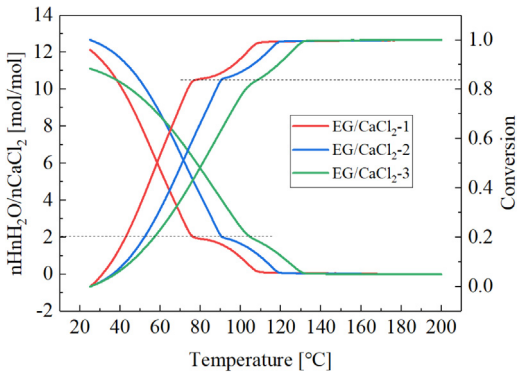

Fig. 7. Water mole content and conversion of EG/$CaCl_2$ composites during dehydration.

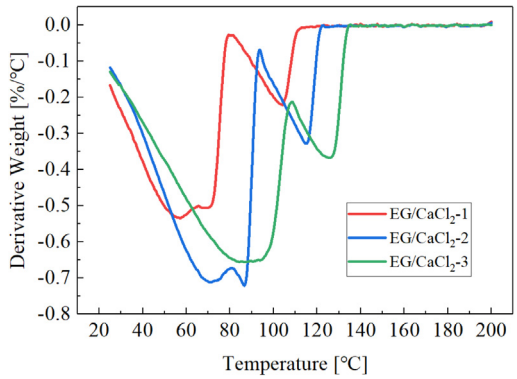

Fig. 8. DTG curves of pure EG and EG/$CaCl_2$ composites during dehydration.

multi-step reactions of $CaCl_2{\cdot}6H_2O$ dehydration into anhydrous $CaCl_2$. Moreover, the peaks are highly overlapped, and the degree of overlap increases with salt content, making it difficult to clarify the weight change and energy storage contribution of each step. Aiming to figure out more quantitative information of this multi-step desorption, peak fitting method was conducted to separate each sub-process. Details are discussed in 3.4.

3.4. Peak fitting approach

To identify mechanism of multi-step desorption for EG/$CaCl_2$ composites, the DTG curves was analyzed using peak fitting approach. Weighing the heat storage potential and salt leakage risk, the curve of sample EG/$CaCl_2$-3 is studied here. Fig. 9 shows five main predicted peaks isolated from the experimental DTG curve: ① desorption of solution absorption water (SW); ② dehydration of $CaCl_2{\cdot}6H_2O$ into $CaCl_2{\cdot}4H_2O$; ③ dehydration of $CaCl_2{\cdot}4H_2O$ into $CaCl_2{\cdot}2H_2O$; ④ dehydration of $CaCl_2{\cdot}2H_2O$ into $CaCl_2{\cdot}H_2O$; and ⑤ dehydration of $CaCl_2{\cdot}2H_2O$ into anhydrous $CaCl_2$. Its easily to find that the first peak occupies a large portion during the whole desorption process, and the temperature range is relatively wider than that of chemical dehydration steps. Peak ②∼⑤ are essentially the removal of chemisorption water, which can be described by the following reactions (Fujioka and Suzuki, 2013):

$$CaCl_2 \cdot 6H_2O\,(s) + \Delta H \Leftrightarrow CaCl_2 \cdot 4H_2O(s) + 2H_2O(g) \quad (12)$$

$$CaCl_2 \cdot 4H_2O\,(s) + \Delta H \Leftrightarrow CaCl_2 \cdot 2H_2O(s) + 2H_2O(g) \quad (13)$$

$$CaCl_2 \cdot 2H_2O\,(s) + \Delta H \Leftrightarrow CaCl_2 \cdot H_2O(s) + H_2O(g) \quad (14)$$

$$CaCl_2 \cdot H_2O\,(s) + \Delta H \Leftrightarrow CaCl_2(s) + H_2O(g) \quad (15)$$

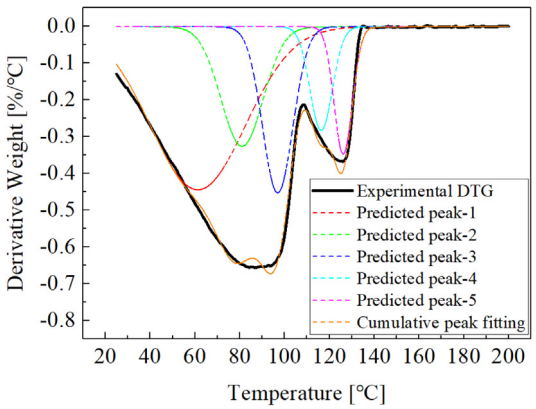

Fig. 9. Experimental DTG curve and predicted peaks for EG/$CaCl_2$-3.

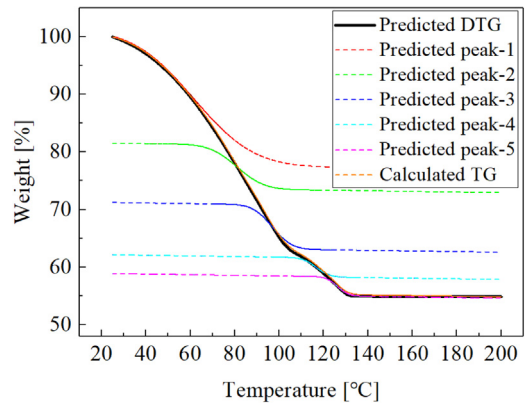

Fig. 10. Experimental and calculated TG curves for EG/$CaCl_2$-3.

It can be seen that the cumulative peak fitting curve is identical to the experimental derivative curve. The predicted curves are converted into TG curves through integration method (Eq. (8)). As shown in Fig. 10, the calculated TG curves coincide well with the experimental TG curve, indicating that the peak fitting data is reliable for reflecting actual desorption process.

By means of the peak fitting analysis, the multi-step desorption process and step weight loss with regards to temperature can be conveniently obtained for each sample. Tables 2–4 summarizes the total weight change measured by TG experiment, the predicted weight changes of each sub-peak and their calculated sums for sample EG/$CaCl_2$-1, EG/$CaCl_2$-2 and EG/$CaCl_2$-3, representatively. The data show that the weight change proportion of the sub-peaks follows a consistent rule for all samples. The weight loss during peak-5, where one crystal water is desorbed from the hydration, makes approximately 8.2%∼8.5% of the total water change. The value is roughly in line with that of peak-4 (8.2%∼8.5%) where one crystal water lost, and also consistent with the result of peak-3 (16.4%∼17.3%) and peak-2 (16.4%∼17.3%) where 2 crystal water desorbed respectively. By combine peak-4 and peak-5 together, we can find that the dehydration process of $CaCl_2{\cdot}2H_2O$ to $CaCl_2$ contributes 16.4%∼17% of the total water change, which is in accordance with the conversion curve (Fig. 7) that implying an 83% completeness of the dehydration when there are only two crystal water left. Moreover, the weight change associate with solution absorption water accounts for nearly half portion (48.4%∼50.5%) of the total water uptake, which would make a significant impact on the overall heat storage performance of the composite.

Table 2
Experimental weight changes and the integral values from peak fitting data.

Curve	Peak temperature (°C)	Weight change (%)	Proportion in total weight change (%)
Experimental TG	–	25.7	–
Calculated sum	–	25.9	100%
Peak-1	44.6	12.5	48.4%
Peak-2	58.9	4.5	17.3%
Peak-3	70.4	4.5	17.3%
Peak-4	94.1	2.2	8.5%
Peak-5	103.4	2.2	8.5%

Table 3
Experimental weight changes and the integral values from peak fitting data.

Curve	Peak temperature (°C)	Weight change (%)	Proportion in total weight change (%)
Experimental TG	–	39.4	–
Calculated sum	–	39.6	100%
Peak-1	56.3	20.0	50.5%
Peak-2	71.4	6.6	16.7%
Peak-3	84.6	6.5	16.4%
Peak-4	106.3	3.3	8.2%
Peak-5	115.2	3.2	8.2%

Table 4
Experimental weight changes and the integral values from peak fitting data.

Curve	Peak temperature (°C)	Weight change (%)	Proportion in total weight change (%)
Experimental TG	–	45.2	–
Calculated sum	–	46.1	100%
Peak-1	61.5	22.7	49.2%
Peak-2	89.0	7.9	17.2%
Peak-3	97.0	7.9	17.2%
Peak-4	116.7	3.8	8.2%
Peak-5	126.2	3.8	8.2%

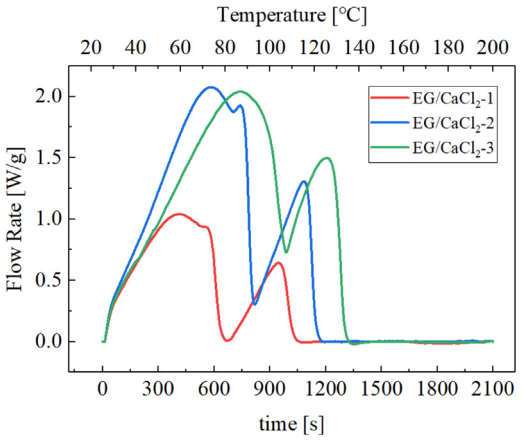

Fig. 11. DSC curve of EG/$CaCl_2$ composites during desorption.

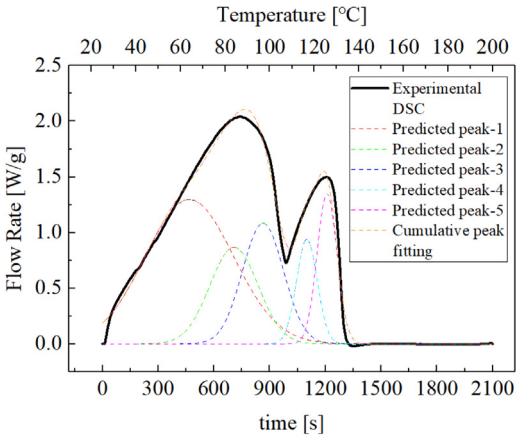

Fig. 12. Peak fitting of DSC curve for EG/$CaCl_2$-3.

3.5. Heat storage capacity

Fig. 11 shows the normalized DSC curves of EG/$CaCl_2$ composites based on the mass of anhydrous sample. The heat flow of composites with different SC values show the similar multi-peak trend, and correspond well with DTG curves (Fig. 8). There are two apparent separated peaks in the DSC curves for each sample, and also one tiny peak for low-SC sample (EG/$CaCl_2$-1 and EG/$CaCl_2$-2). It has been known from Section 3.4 that the first apparent peak is actually a combined peak consisting of three sub-peaks including solution desorption and chemical desorption ($CaCl_2{\cdot}6H_2O \rightarrow CaCl_2{\cdot}6H_2O \rightarrow CaCl_2{\cdot}2H_2O$). And the second apparent peak is composed two sub-peaks which imply a two-step desorption of $CaCl_2{\cdot}2H_2O$ into anhydrous $CaCl_2$. The overlapping between sub-peaks increases with the salt content of sample increases, meanwhile separation degree between the two apparent peaks decrease. Overall, a highest heat storage capacity of 1637.6 kJ/kg is obtained for EG/$CaCl_2$-3 with a water uptake of 0.79 g/g (Fig. 5). For the other two samples with lower salt content, the heat storage capacity turned out to be 581.5 kJ/kg (EG/$CaCl_2$-1) and 1372.0 kJ/kg (EG/$CaCl_2$-2).

Peak fitting approach is conducted for DSC curve of EG/$CaCl_2$-3 (Fig. 12) for a comparable analysis with DTG peak fitting in 3.4. Locations and widths of the sub-peaks are set in line with that of predicted DTG sub-peaks (Fig. 9). Heat storage performance during the predicted sub-processes are obtained by integral method, and the results are summarized in Table 5. The cumulative peak fitting curve is identical to the experimental derivative curve, with a small deviation of 0.6%. The data show that solution desorption accounts for about 45.8% of the total heat storage capacity, which plays nearly the equitant important role as the chemical sorption. Proportion of the chemisorption peaks contribute to the total chemical adsorption by 31.6% (peak-2), 33.6% (peak-3), 14.6% (peak-4), 20.2% (peak-5), respectively, showing good consistency with the theoretical reaction enthalpy (Eqs. (12)∼(15)) calculated from formation enthalpy values (Company, 2003), confirming the reliability and accuracy of the prediction result. The last two peaks are relatively easier to be separated from the previous peaks by the critical point around 110 °C, which account for approximately only 20% (230.3 kJ/kg) of the total heat storage capacity while occupying about 19% of the operation period. Therefore, for low-grade heat within 110 °C, similar heat storage efficiency is achievable for by confine the desorption process to the first three peaks. In conclusion, with the assistant analysis by peak fitting approach, one can easily clarify the multi-form sorption mechanism from normal TG or DSC measurement, and thus control the operation condition for a stable running state and a maximum efficiency for a heat storage system.

4. Conclusions

The heat storage performance of EG/$CaCl_2$ composites was investigated in this study. TG measurements suggest that all samples show a quite high reactivity of desorption within 130 °C, indicating the great potential of EG/$CaCl_2$ composite for low-grade heat storage. The best heat storage capacity of 1637.6 kJ/kg

Table 5
Peak fitting data of heat storage performance and dehydration enthalpy.

Curve	Temperature range (°C)	Predicted heat storage (J/g)	Proportion in total heat storage (%)	Thermochemical heat storage		
				Predicted proportion (%)	Theoretical proportion (%)	Theoretical reaction enthalpy (kJ/mol)
Experimental DSC	25.0∼133.2	1637.6	–	–	–	–
Calculated sum	–	1647.0	100	100	100	361.6
Peak-1	24.3∼103.7	753.7	45.8	–	–	–
Peak-2	62.3∼105.6	282.0	17.1	31.6	31.7	114.7
Peak-3	78.5∼115.5	300.0	18.2	33.6	33.7	121.9
Peak-4	107.4∼126.0	130.9	7.9	14.6	14.2	51.4
Peak-5	116.8∼134.6	180.4	11.0	20.2	20.4	73.6

was obtained for the composite EG/$CaCl_2$-3 (48.1 wt%), with a water uptake of 0.79 g/g.

Water sorption/desorption behaviors were examined in detail to reveal the multi-form heat storage mechanism. The high porosity and lamellar structure of host EG matrix guarantee a good sorption capacity much higher than pure salt hydration ($CaCl_2 \rightarrow CaCl_2{\cdot}6H_2O$). Peak fitting analysis of TG curve shows that solution absorption contributes to nearly a half (48.4%∼50.5%) of the total water uptake, which is similar to the share of chemisorption (49.5%∼51.6%). For the composite with best heat storage capacity, EG/$CaCl_2$-3, the corresponding proportion of heat storage are 45.8% (solution desorption) and 54.2% (chemical dehydration). From this view of point, the deliquescence is beneficial for improving performance of the heat storage, thus supporting ability of host matrix is important for improving the heat storage capacity of composite material.

Through the novel prediction method combining peak fitting approach and TG/DSC measurements, sub-steps during desorption process can be easily clarified with less experimental resources. The reliability and accuracy of the prediction results can be confirmed on the basis of experiment data and theoretical calculation. The dehydration process in this study is predicted to contain five main steps: ① solution desorption; ② dehydration of $CaCl_2{\cdot}6H_2O$ into $CaCl_2{\cdot}4H_2O$; ③ dehydration of $CaCl_2{\cdot}4H_2O$ into $CaCl_2{\cdot}2H_2O$; ④ dehydration of $CaCl_2{\cdot}2H_2O$ into $CaCl_2{\cdot}2H_2O$; and ⑤ dehydration of $CaCl_2{\cdot}H_2O$ into anhydrous $CaCl_2$. The results show good consistency with TG/DSC curves and reaction enthalpy values, and offer theoretical basis of material design and operation control for a maximum heat storage performance. Future studies should focus on kinetics characteristics of EG/$CaCl_2$ composites based on this five-step mechanism, and on the cyclic stability which might deteriorate because of deliquesce.

CRediT authorship contribution statement

Na Gao: Conceptualization, Methodology, Investigation, Formal analysis, Writing – original draft. **Lisheng Deng:** Conceptualization, Data curation, Writing – review & editing. **Jun Li:** Validation, Methodology. **Hongyu Huang:** Supervision, Funding acquisition, Writing – review & editing. **Bin Zhou:** Investigation. **You Zhou:** Resource, Supervision, Funding acquisition.

Declaration of competing interest

The authors declare that they have no known competing financial interests or personal relationships that could have appeared to influence the work reported in this paper.

Data availability

Data will be made available on request.

Acknowledgments

This work was supported by Key Area Research and Development Program of Guangdong Province, China (2019B110209003), Key Special Project for Introduced Talents Team of Southern Marine Science and Engineering Guangdong Laboratory (Guangzhou), China (GML2019ZD0108) and Technology project of China Energy Investment Corporation, China (GJNY-20-121).

References

Ait Ousaleh, H., et al., 2020. New hybrid graphene/inorganic salt composites for thermochemical energy storage: Synthesis, cyclability investigation and heat exchanger metal corrosion protection performance. Sol. Energy Mater. Sol. Cells 215.
Angerer, Michael, et al., 2018. Design of a MW-scale thermo-chemical energy storage reactor. Energy Rep. 4, 507–519.
Ao, Ci, et al., 2022. Stearic acid/expanded graphite composite phase change material with high thermal conductivity for thermal energy storage. Energy Rep. 8, 4834–4843.
Calabrese, L., et al., 2019. Magnesium sulphate-silicone foam composites for thermochemical energy storage: Assessment of dehydration behaviour and mechanical stability. Sol. Energy Mater. Sol. Cells 200.
Company, The Dow Chemical, 2003. Calcium Chloride Handbook. United States.
Courbon, E., et al., 2017. Further improvement of the synthesis of silica gel and $CaCl_2$ composites: Enhancement of energy storage density and stability over cycles for solar heat storage coupled with space heating applications. Sol. Energy 157, 532–541.
Ding, Zhixiong, et al., 2022. On the rational development of advanced thermochemical thermal batteries for short-term and long-term energy storage. Renew. Sustain. Energy Rev. 164, 112557.
Esaki, Takehiro, Kobayashi, Noriyuki, 2020. Study on the cycle characteristics of chemical heat storage with different reactor module types for calcium chloride hydration. Appl. Therm. Eng. 171, 114988.
Forman, Clemens, et al., 2016. Estimating the global waste heat potential. Renew. Sustain. Energy Rev. 57, 1568–1579.
Fujioka, Keiko, Suzuki, Hiroshi, 2013. Thermophysical properties and reaction rate of composite reactant of calcium chloride and expanded graphite. Appl. Therm. Eng. 50, 1627–1632.
Gollsch, M., et al., 2020. Investigation of calcium hydroxide powder for thermochemical storage modified with nanostructured flow agents. Sol. Energy 201, 810–818.
Haruki, Masashi, et al., 2019. Thermal conductivity and reactivity of $Mg(OH)_2$ and MgO/expanded graphite composites with high packing density for chemical heat storage. Thermochim. Acta 680, 178338.
Haruki, M., et al., 2020. Effect of combining with thermally expanded graphite on thermal conductivities of the lanthanum sulfate hydrate types of chemical heat storage material. Mater. Chem. Phys. 252.
Jabbari-Hichri, Amira, et al., 2017. $CaCl_2$-containing composites as thermochemical heat storage materials. Sol. Energy Mater. Sol. Cells 172, 177–185.
Janković, Bojan, et al., 2018. TSA-MS characterization and kinetic study of the pyrolysis process of various types of biomass based on the Gaussian multi-peak fitting and peak-to-peak approaches. Fuel 234, 447–463.
Kim, Seon Tae, et al., 2014. The optimization of mixing ratio of expanded graphite mixed chemical heat storage material for magnesium oxide/water chemical heat pump. Appl. Therm. Eng. 66, 274–281.
Kimpton, Harriet, et al., 2020. Decarbonising heating and hot water using solar thermal collectors coupled with thermal storage: The scale of the challenge. Energy Rep. 6, 25–34.
Kubota, M., et al., 2019. Enhancement of hydration rate of LiOH by combining with mesoporous carbon for Low-temperature chemical heat storage. Appl. Therm. Eng. 150, 858–863.

Li, Wei, et al., 2021. Characterisation and sorption behaviour of LiOH-LiCl@EG composite sorbents for thermochemical energy storage with controllable thermal upgradeability. Chem. Eng. J. 421, 129586.
Linder, Marc, 2021. 16 - Using thermochemical reactions in thermal energy storage systems. In: Cabeza, Luisa F. (Ed.), Advances in Thermal Energy Storage Systems (Second Edition). Woodhead Publishing.
Liu, Xin, et al., 2022. Development of $MgSO_4$/mesoporous silica composites for thermochemical energy storage: the role of porous structure on water adsorption. Energy Rep. 8, 4913–4921.
Mastronardo, E., et al., 2016. Thermochemical performance of carbon nanotubes based hybrid materials for $MgO/H_2O/Mg(OH)_2$ chemical heat pumps. Appl. Energy 181, 232–243.
Miao, Qi, et al., 2021. $MgSO_4$-expanded graphite composites for mass and heat transfer enhancement of thermochemical energy storage. Sol. Energy 220, 432–439.
Molenda, Margarethe, et al., 2013. Reversible hydration behavior of $CaCl_2$ at high H_2O partial pressures for thermochemical energy storage. Thermochim. Acta 560, 76–81.
Nonnen, T., et al., 2020. Salt inclusion and deliquescence in salt/zeolite X composites for thermochemical heat storage. Microporous Mesoporous Mater. 303, 110239.
N'Tsoukpoe, Kokouvi Edem, et al., 2014. A systematic multi-step screening of numerous salt hydrates for low temperature thermochemical energy storage. Appl. Energy 124, 1–16.
Owusu-Ware, Samuel K., et al., 2013. Quantitative analysis of overlapping processes in the non-isothermal decomposition of chlorogenic acid by peak fitting. Thermochim. Acta 565, 27–33.
Posern, K., Osburg, A., 2018. Determination of the heat storage performance of thermochemical heat storage materials based on $SrCl_2$ and $MgSO_4$. J. Therm. Anal. Calorim. 131, 2769–2773.
Rammelberg, Holger Urs, et al., 2012. Hydration and dehydration of salt hydrates and hydroxides for thermal energy storage - kinetics and energy release. Energy Procedia 30, 362–369.
Richter, M., et al., 2018. A systematic screening of salt hydrates as materials for a thermochemical heat transformer. Thermochim. Acta 659, 136–150.
Ristić, Alenka, Logar, Nataša Zabukovec, 2019. New composite water sorbents $CaCl_2$-PHTS for low-temperature sorption heat storage: Determination of structural properties. Nanomaterials 9 (27).
Ristić, Alenka, et al., 2012. New two-component water sorbent $CaCl_2$-FeKIL2 for solar thermal energy storage. Microporous Mesoporous Mater. 164, 266–272.
Skrylnyk, O., et al., 2018. Performance characterization of salt-in-silica composite materials for seasonal energy storage design. J. Energy Storage 19, 320–336.
Stengler, Jana, et al., 2020. Thermodynamic and kinetic investigations of the $SrBr_2$ hydration and dehydration reactions for thermochemical energy storage and heat transformation. Appl. Energy 277, 115432.
Touloumet, Quentin, et al., 2021. Water sorption and heat storage in $CaCl_2$ impregnated aluminium fumarate MOFs. Sol. Energy Mater. Sol. Cells 231, 111332.
Touloumet, Quentin, et al., 2022. Hierarchical aluminum fumarate metal–organic framework - alumina host matrix: Design and application to $CaCl_2$ composites for thermochemical heat storage. J. Energy Storage 50, 104702.
Veith, Heiner, et al., 2021. Predicting deliquescence relative humidities of crystals and crystal mixtures. Molecules 26 (3176).
Wang, Q., et al., 2019. Structure and hydration state characterizations of $MgSO_4$-zeolite 13x composite materials for long-term thermochemical heat storage. Sol. Energy Mater. Sol. Cells 200.
Wolf, Veronika, et al., 2022. Analysis of the thermodynamic performance of transcritical CO_2 power cycle configurations for low grade waste heat recovery. Energy Rep. 8, 4196–4208.
Xin, Yixiu, et al., 2022. Effect of NiCo2O4-modified expanded graphite on heat transfer and storage improvement of $CaCl_2$·6H2O. J. Energy Storage 46, 103902.
Xing, Baoyan, et al., 2022. Hybrid composite materials generated via growth of carbon nanotubes in expanded graphite pores using a microwave technique. Inorg. Chem. Commun. 137, 109185.
Xu, J.X., et al., 2019. High energy-density multi-form thermochemical energy storage based on multi-step sorption processes. Energy 185, 1131–1142.
Xueling, Zhang, et al., 2021. Heat storage performance analysis of ZMS-Porous media/$CaCl_2$/$MgSO_4$ composite thermochemical heat storage materials. Sol. Energy Mater. Sol. Cells 230, 111246.
Yan, T., et al., 2015. A review of promising candidate reactions for chemical heat storage. Renew. Sustain. Energy Rev. 43, 13–31.
Yilmaz, B., et al., 2020. Synthesis and characterization of salt-impregnated anodic aluminum oxide composites for low-grade heat storage. Int. J. Miner. Metall. Mater. 27, 112–118.
Zamengo, Massimiliano, et al., 2015. Chemical heat storage of thermal energy from a nuclear reactor by using a magnesium hydroxide/expanded graphite composite material. Energy Procedia 71, 293–305.
Zhang, Y., et al., 2016. Thermochemical characterizations of novel vermiculite-LiCl composite sorbents for low-temperature heat storage. Energies 9.
Zhou, Hong, Zhang, Dong, 2022. Investigation on pH/temperature-manipulated hydrothermally reduced graphene oxide aerogel impregnated with $MgCl_2$ hydrates for low-temperature thermochemical heat storage. Sol. Energy Mater. Sol. Cells 241, 111740.